On Non-Geostrophic Baroclinic Stability: Part II

PETER H. STONE

Division of Engineering and Applied Physics, Harvard University, Cambridge, Mass.

(Manuscript received 26 February 1970)

ABSTRACT

The solutions of Eady's 1949 model of baroclinic stability are extended numerically to include the non-geostrophic perturbations which were not covered by the analysis in Part I. It is found that the largest growth rates are never associated with these new perturbations, so the tentative conclusions of Part I are verified. The more exact numerical solutions lead only to slight quantitative modifications of the results of Part I. If we let Ri be the Richardson number, then the largest growth rates are associated with "geostrophic" baroclinic instability if $\mathrm{Ri}>0.950$; with symmetric instability if $\frac{1}{4}<\mathrm{Ri}<0.950$; and with Kelvin-Helmholtz instability if $0<\mathrm{Ri}<\frac{1}{4}$. Geostrophic baroclinic instability and symmetric instability can exist simultaneously if $0.84<\mathrm{Ri}<1$, and symmetric instability and Kelvin-Helmholtz instability can exist simultaneously if $0<\mathrm{Ri}<\frac{1}{4}$.

1. Introduction

In an earlier study [Stone (1966) hereinafter referred to as Part I], Eady's (1949) model of baroclinic flow was used to determine the growth rates of non-geostrophic perturbations of a thermal wind. The nature of the mathematical approximations used in Part I restricted the horizontal scales of the perturbations, so that not all non-geostrophic perturbations were included in the analysis. In particular, growth rates were not found for those perturbations whose horizontal scales were such that the two Rossby numbers defined using the zonal and meridional length scales were both of order unity (see Fig. 5 in Part I). The growth rates for the other perturbations showed that there were three different types of perturbations which could have the largest growth rates. These three different types of perturbations are each associated with one of three different types of instability well known from earlier work; namely, geostrophic baroclinic instability (e.g., Eady, 1949), symmetric instability (e.g., Solberg, 1936), and Kelvin-Helmholtz instability (e.g., Chandrasekhar, 1961). Which type of instability has the largest growth rates depends on the Richardson number, Ri. The results of Part I indicated that the largest growth rates are associated with baroclinic instability if $\mathrm{Ri}>0.95$; with symmetric instability if $\frac{1}{4}<\mathrm{Ri}<0.95$; and with Kelvin-Helmholtz instability if $0<\mathrm{Ri}<\frac{1}{4}$.

If there should be some values of Ri for which the largest growth rates were associated with the perturbations not covered by the analysis in Part I, then the above picture would have to be modified. A more recent analysis by Orlanski (1968) used a different model in determining the growth rates of non-geostrophic perturbations. In his model the vertical shear of the flow was entirely concentrated in a frontal discontinuity, in contrast to Eady's model where the vertical shear is uniform. Orlanski's results did include perturbations of the kind not included in Part I, but he did not find any essentially different maxima in the growth rate. (His results did include maxima corresponding to barotropic instability because his frontal surface was not horizontal; this type of instability, however, is automatically excluded in Eady's model by the neglect of any cross-stream variation in the unperturbed wind.) On the other hand, Orlanski's model automatically excluded symmetric instability, because the motions associated with this type of instability are parallel to the isotherms of potential temperature, and such motions are not resolved when all the isotherms are concentrated into a single surface of discontinuity. However, it is just when the growth rates of symmetric and baroclinic instabilities are comparable, i.e., when $\mathrm{Ri}\approx 1$, that the possibility of the maximum growth rate being associated with the neglected perturbations is strongest. The growth rate maxima found in Part I were not sharply peaked in this range, and the selectivity of different perturbations was very weak. Thus, Orlanski's results leave open the possibility of a different growth rate maximum, associated with a basically different kind of perturbation, in the baroclinic flow problem with uniform shear. To resolve this possibility, in this paper we extend the analysis of Part I to include the non-geostrophic perturbations previously left out.

2. Mathematical model

As in Part I, we will use Eady's model of baroclinic stability. Let H be the depth of the fluid; u_0 the magnitude of the thermal wind; f the Coriolis parameter; x, y and z the dimensionless zonal, meridional and vertical coordinates (x and y are measured in units of u_0/f and z in units of H); u, v and w the corresponding

dimensionless velocity components (u and v measured in units of u_0 and w measured in units of fH); t the dimensionless time coordinate (measured in units of $1/f$); and θ the dimensionless potential temperature (measured in units of the total vertical range $\Delta\theta$ of potential temperature).

In Eady's model, effects of dissipation and curvature are neglected, and the Boussinesq approximation is used for compressibility effects. The unperturbed wind and temperature fields satisfy the thermal wind relation and have the forms

$$\left.\begin{aligned} u&=z \\ v&=w=0 \\ \theta&=z-\frac{1}{\mathrm{Ri}}y+\frac{\theta_0}{\Delta\theta}-\tfrac{1}{2} \end{aligned}\right\}, \tag{2.1}$$

where

$$\mathrm{Ri}=\frac{gH}{u_0^2}\frac{\Delta\theta}{\theta_0}, \tag{2.2}$$

g is the gravitational acceleration, and θ_0 the average potential temperature. The perturbations of the above flow field are assumed to be small and to have x, y and t dependences of the form $\exp[i(\sigma t+kx+\lambda y)]$, where σ is a complex frequency, and k and λ are the zonal and meridional wavenumbers, respectively. If we use a bar to denote the same quantities with dimensions, then

$$\left.\begin{aligned} \sigma&=\frac{\bar{\sigma}}{f} \\ k&=\frac{u_0\bar{k}}{f} \\ \lambda&=\frac{u_0\bar{\lambda}}{f} \end{aligned}\right\}. \tag{2.3}$$

Therefore, k and λ can be interpreted directly as the zonal and meridional Rossby numbers of the perturbation. The resulting eigenvalue problem is [see Eady (1949, Eq. (11), Section II)]

$$[1-(\sigma+kz)^2]\frac{d^2w}{dz^2}-\left[\frac{2k}{\sigma+kz}-2i\lambda\right]\frac{dw}{dz}-\left[\mathrm{Ri}(k^2+\lambda^2)+\frac{2ik\lambda}{\sigma+kz}\right]w=0, \tag{2.4}$$

with

$$w=0, \quad \text{when} \quad z=0,\ 1, \tag{2.5}$$

w being the z-dependent part of the perturbation vertical velocity.

Perturbations such that k, $\lambda\approx 1$ were not included in the analysis of Part I. Growth rates for the other perturbations were found by expanding the solution to (2.4) and (2.5) in power series of k and λ or their inverses. In the more difficult case when k, $\lambda\approx 1$ we shall have to use numerical techniques. For this purpose it is convenient to rewrite Eq. (2.4) in normal form. Let

$$w=\frac{h}{\sqrt{1-h^2}}\left(\frac{1-h}{1+h}\right)^{i\lambda/(2k)}\phi, \tag{2.6}$$

where $h=\sigma+kz$. Substituting (2.6) into (2.4) and (2.5), we obtain

$$\frac{d^2\phi}{dz^2}+a(z)\phi=0, \tag{2.7}$$

$$\phi=0, \quad \text{on} \quad z=0,\ 1, \tag{2.8}$$

where

$$a(z)=\frac{k^2[\mathrm{Ri}h^4+(3-\mathrm{Ri})h^2-2]+\lambda^2[\mathrm{Ri}h^4+(1-\mathrm{Ri})h^2]}{h^2(1-h^2)^2}. \tag{2.9}$$

3. Method of solution

Eq. (2.7) was replaced by a set of simple difference equations

$$\phi_{n+1}-2\left(1-\frac{\Delta^2}{2}a_n\right)\phi_n+\phi_{n-1}=0, \quad n=1,2,3,\cdots,N, \tag{3.1}$$

where

$$\left.\begin{aligned} \Delta&=\frac{1}{N+1} \\ \phi_n&=\phi(z_n) \\ a_n&=a(z_n) \\ z_n&=n\Delta \end{aligned}\right\}. \tag{3.2}$$

Large values of N were relied on to obtain sufficient accuracy. In general, $N=100$ was used, a value more than ample to obtain 0.1% accuracy.

The eigenvalue σ was determined by an iterative procedure, using a CDC 6400 computer. For given values of k, λ, Ri, an initial guess for σ was made. Because of the boundary conditions (2.8), $\phi_0=0$, and the amplitude of the eigenfunction was set by choosing $\phi_1=1$. Thus, it was possible to solve Eqs. (3.1) successively for $\phi_2, \phi_3, \cdots, \phi_{N+1}$. In general, the guess for σ is incorrect and the calculated value for ϕ_{N+1} will not be zero, although it should be according to boundary condition (2.8). Consequently, the calculation of ϕ_{N+1} was repeated, using a value of σ which differed from the

initial guess by a small quantity ϵ. The two values of ϕ_{N+1} were then used to perform a linear extrapolation from the two values of σ to a new value of σ which would make ϕ_{N+1} zero if it depended on σ in a linear fashion. The new value of σ was then used to reiterate the whole procedure, and as many iterations were performed as was necessary to get a final value of σ accurate to 0.1%.

A numerical integration such as the above will not work if one is interested in finding the real values of σ, since then the coefficient $a(z)$ is, in general, singular within the range of integration. This was not a problem for this study, since the complex, unstable values of σ were sought. For small values of k, the initial guesses for σ were taken from the approximate results of Part I. For larger values of k the initial guess was taken to be the value of σ for the nearest value of k available. For $k \lesssim 1$ three or four iterations were generally sufficient to obtain σ with 0.1% accuracy. The number of iterations necessary increased for larger values of k, and in fact for $k \gtrsim 10$ the iterations gave diverging values for σ. This divergence was due to the extreme sensitivity of the calculation of ϕ_{N+1} to small changes in σ when $k \gg 1$. Consequently, round-off error was sufficient to give random fluctuations in the calculated values of ϕ_{N+1}. In any case the values for $k \gtrsim 10$ were not of prime interest since the asymptotic solutions as $k \to \infty$ were found in Part I. Comparison of the numerical solutions with the asymptotic solutions when their regions of validity overlapped showed agreement within the limits of the approximations.

4. Numerical results

Fig. 1 shows the growth rates of the perturbations as functions of the zonal wavenumber for various values of λ, when Ri=2. The behavior of the eigenvalues for this value of Ri is typical of the behavior for all larger values of Ri, and is qualitatively the same behavior as in Eady's solution for Ri$\gg$1. The maximum growth rate occurs when λ=0, and corresponds to "geostrophic" baroclinic instability, although the most rapidly growing perturbations are non-geostrophic when Ri$\approx$1. The perturbations are stable when λ or k are sufficiently

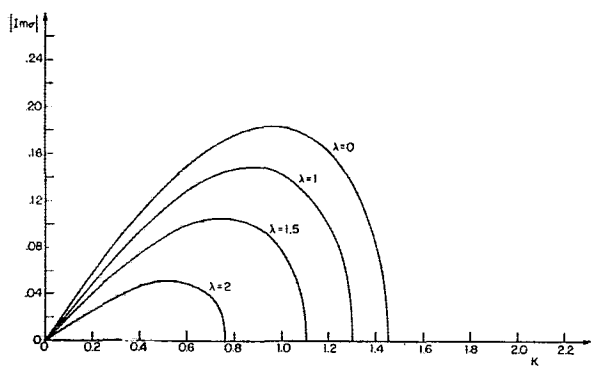

FIG. 1. Growth rates vs k when Ri=2.

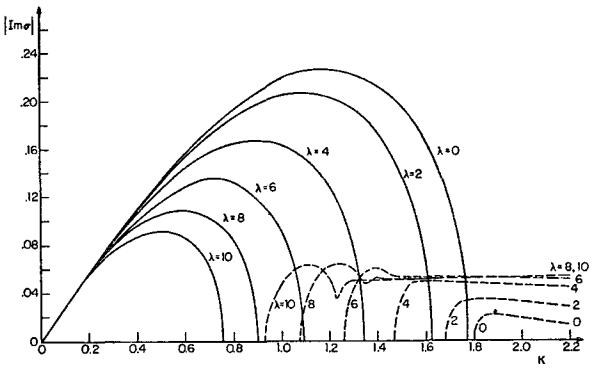

FIG. 2. Growth rates when Ri=1.

large, and the unstable perturbations all have phase speeds c ($=-\mathrm{Re}\sigma/k$) equal to $\frac{1}{2}$.

Fig. 2 shows the growth rates for the critical value Ri=1. This is the largest value of Ri for which unstable perturbations exist for all values of λ. In addition, for a given value of λ, there are now two sets of unstable perturbations. Those for small values of k (given by the solid curves in Fig. 2) are the analytic continuation of the geostrophic baroclinic instabilities. Those for large values of k (given by the dashed curves in Fig. 2) have smaller growth rates. These latter, small-scale perturbations have growth rates which decrease as Ri increases, and may in fact still be unstable for Ri$\gtrsim$2, but if so the growth rates were too small to be found by our numerical method, because of the near singular behavior of the coefficients of the differential equation when Imσ is very small.

When Ri<1, there is more than one unstable eigenmode [see Part I, Eq. (2.27)]. The most unstable one is the analytic continuation of the single unstable mode when Ri>1, and it is illustrated in Fig. 3 for Ri=0.92. Now the maximum growth rate corresponding to symmetric instability (k=0, $\lambda \gg 1$) is apparent. At the same time the maximum corresponding to geostrophic baroclinic instability is still present. The numerical computations showed that the two maxima have equal growth rates when Ri=0.950. (This may be contrasted with the approximate value Ri=0.95 found in Part I.) For smaller values of Ri the symmetric maximum is greater.

In Fig. 3 we also see that the unstable perturbations for large k (again indicated by the dashed curves) in fact join on to the unstable perturbations for small k. Only for some values of Ri and λ is there an intermediate range of k which is stable, and this tends to obscure the fact that the solid and dashed curves in the figures are really analytic continuations of the same eigenvalue. The maximum growth rate associated with these smaller scale perturbations is still smaller than those associated with the other perturbations.

The numerical results confirm the conclusion of Part I that the first mode (the one with the fewest zeros

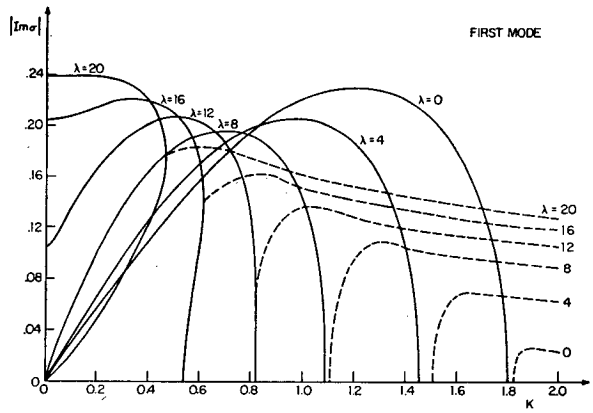

FIG. 3. Growth rates for the most unstable mode when Ri=0.92.

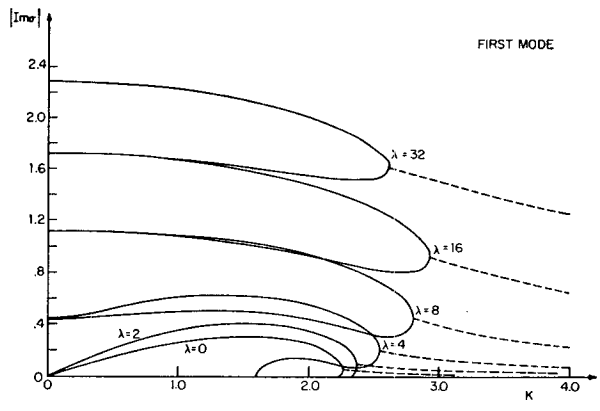

FIG. 5. Growth rates for the most unstable mode when Ri=0.1.

between $z=0$ and $z=1$) is always the most unstable. They also show that the set of unstable modes, found in Part I when $k\ll 1$ and λ is sufficiently large, join together in pairs when $k\approx 1$. For example, the two most unstable modes when $k\ll 1$ join together when $k\approx 1$ as shown by the curve for $\lambda=20$ in Fig. 3. Similarly, the third and fourth most unstable modes join together when $k\approx 1$, etc., for the higher modes. There can also be more than one unstable eigenmode for intermediate values of k, even though there is not for small k (see the curve for $\lambda=16$ in Fig. 3).

Figs. 4 and 5 show the growth rates for the most unstable mode when Ri=0.5 and 0.1. Now the only growth rate maximum is that corresponding to the symmetric perturbations. (The Kelvin-Helmholtz maximum when $\mathrm{Ri}<\frac{1}{4}$ occurs when $k\gg 1$—see Part I, Section 5.) There are no longer any values of λ for which there exists an intermediate range of k where the perturbations are stable. Computations for intermediate values of Ri show that the maximum corresponding to geostrophic baroclinic instability disappears when Ri decreases to 0.84. (This value may be compared with the approximate value 0.75 found in Part I.) When Ri<0.84, this latter maximum is replaced by a saddle point in the k, λ plane.

Figs. 6 and 7 show the typical behavior of the real part of σ when Ri<1. Both the real and imaginary parts, σ_r and σ_i, are plotted for comparison. These values may be combined with any sign to form an eigenvalue, i.e., $\pm\sigma_r\pm i\sigma_i$ are all eigenvalues for the problem. Aside from the choice of signs, there are, in general, an infinite number of distinct eigenvalues. The most unstable pair, i.e., the same pair as is illustrated in Figs. 4 and 5, is shown in Figs. 6 and 7 for particular values of Ri and λ. For small values of k the pair have the same phase speed ($c=\frac{1}{2}$) but different growth rates. For large values of k they have the same growth rate but different phase speeds. As $k\to\infty$, this pair joins onto the asymptotic pair of eigenvalues $\sigma=0$, k (see Section 5 of Part I).

Figs. 8 and 9 illustrate the growth rates for the second most unstable pair of eigenvalues. The two distinct growth rates apparent for a given value of λ

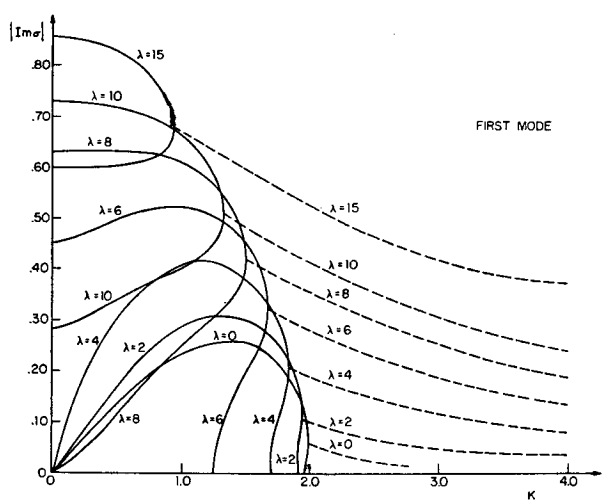

FIG. 4. Growth rates for the most unstable mode when Ri=0.5.

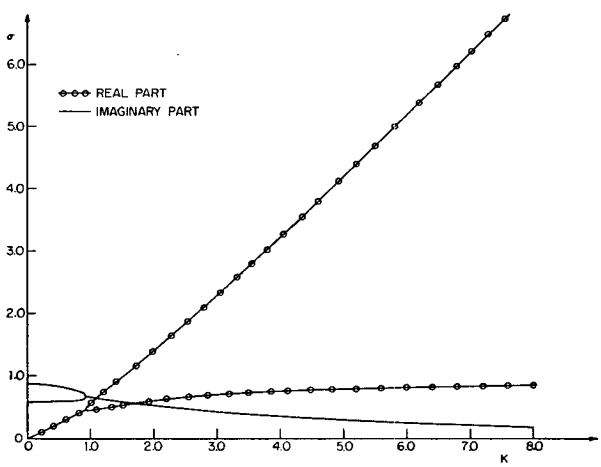

FIG. 6. Real and imaginary parts of σ when $\lambda=15$, Ri=0.5.

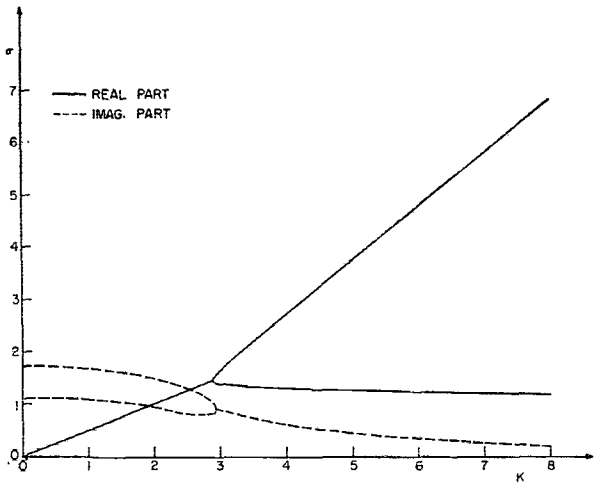

FIG. 7. Real and imaginary parts of σ when $\lambda=16$, Ri$=0.1$.

when $k\ll 1$ correspond to the third and fourth most unstable eigenmodes found in Part I, but here we refer to them collectively as the second mode since they join together when $k\approx 1$. The dependence of the growth rates on k, λ and Ri is similar to that for the first mode, except that the growth rates go to zero for sufficiently small values of λ, and there is never a maximum analogous to the geostrophic baroclinic maximum. The eigenvalues of the second and higher modes join on to the other asymptotic solutions found in Part I [Eq. (5.4)] when $k\gg 1$.

Finally, we can compare the approximate expression for the growth rates of the geostrophic baroclinic instabilities found in Part I [Eq. (4.25)] with the exact numerical results. The approximate formula, when $\lambda=0$, is

$$\sigma_i=\frac{k}{2\sqrt{3}}\left[1-\frac{2k^2}{15}(1+\mathrm{Ri})\right]. \tag{4.1}$$

According to this formula the most unstable zonal wavenumber is

$$k=\left(\frac{5/2}{1+\mathrm{Ri}}\right)^{\frac{1}{2}}, \tag{4.2}$$

and it has a growth rate

$$\sigma_i=\left(\frac{5/54}{1+\mathrm{Ri}}\right)^{\frac{1}{2}}. \tag{4.3}$$

Eq. (4.1) is plotted in Fig. 10 along with the exact numerical results for the large-scale perturbations. The curves are plotted for Ri$=\frac{1}{2}$, 1 and 2. [The error in Eq. (4.1) is largest when Ri≈ 1.] The agreement between the two sets of curves is quite good. The error in Eq. (4.2) is never more than 7% and that in Eq. (4.3) never more than 6%.

Eq. (4.2) leads to a simple relation between the zonal scale of the most unstable geostrophic baroclinic perturbation and the internal scales in Eady's model. There are two internal scales: first, the scale we used to put the equations in dimensionless form, i.e.,

$$L_0=\frac{u_0}{f}; \tag{4.4}$$

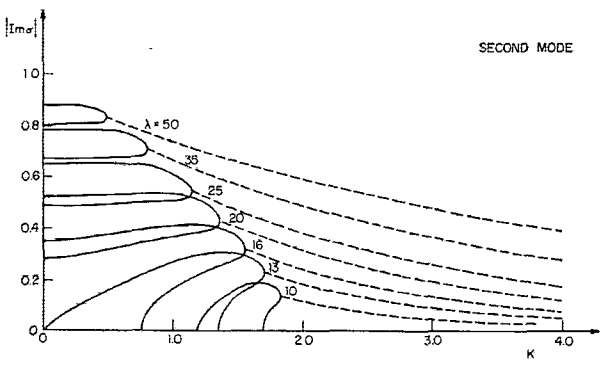

FIG. 8. Growth rates for the second most unstable mode when Ri$=0.5$.

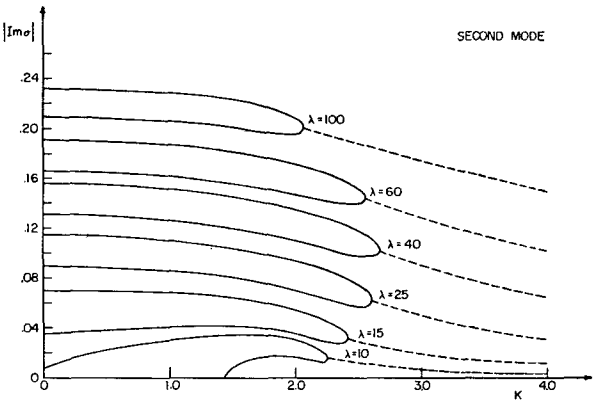

FIG. 9. Growth rates for the second most unstable mode when Ri$=0.1$.

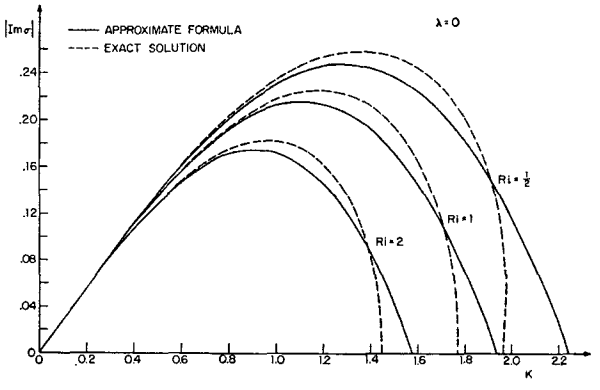

FIG. 10. Comparison of growth rates from the exact and approximate solutions.

and second, the radius of deformation,

$$L_r=\left(\frac{gH}{f^2}\frac{\Delta\theta}{\theta_0}\right)^{\frac{1}{2}}. \tag{4.5}$$

The Richardson number [Eq. (2.2)] can be simply expressed as

$$\mathrm{Ri}=\frac{L_r^2}{L_0^2}. \tag{4.6}$$

Thus, if we let L be the most unstable zonal wavelength with dimensions

$$L=L_0\frac{2\pi}{k}, \tag{4.7}$$

from Eqs. (4.2), (4.6) and (4.7), we obtain

$$L=\frac{2\pi}{\sqrt{5/2}}(L_0^2+L_r^2)^{\frac{1}{2}}=4.0(L_0^2+L_r^2)^{\frac{1}{2}}. \tag{4.8}$$

The zonal scale is simply the root mean square of the two internal scales.

5. Conclusions

The numerical solutions show that the largest growth rates are never associated with the perturbations left out of the analysis of Part I. Therefore, the tentative conclusions of Part I as to which kinds of instability will dominate are verified. The largest growth rates are associated with geostrophic baroclinic instability if $\mathrm{Ri}>0.950$; with symmetric instability if $\frac{1}{4}<\mathrm{Ri}<0.950$; and with Kelvin-Helmholtz instability if $0<\mathrm{Ri}<\frac{1}{4}$. The first two types of instability exist simultaneously if $0.84<\mathrm{Ri}<1$, and the last two types exist simultaneously if $0<\mathrm{Ri}<\frac{1}{4}$. A recent laboratory experiment (Stone, *et al.*, 1969) showed qualitative behavior very similar to these theoretical results.

Acknowledgments. I am indebted to Miss Elaine Beede for carrying out the programming for the numerical computations, and to the Department of Astro-Geophysics at the University of Colorado for their hospitality while this paper was being written. This research was supported in part by the Atmospheric Sciences Section, National Science Foundation, under Grant GP4293 to Harvard University, and in part by a grant from the Alfred P. Sloan Foundation.

REFERENCES

Chandrasekhar, S., 1961: *Hydrodynamic and Hydromagnetic Stability*. Oxford, Clarendon Press, 654 pp.

Eady, E. T., 1949: Long waves and cyclone waves. *Tellus*, **1**, No. 3, 33–52.

Orlanski, I., 1968: Instability of frontal waves. *J. Atmos. Sci.*, **25**, 178–200.

Solberg, H., 1936: Le mouvement d'inertie de l'atmosphère stable et son rôle dans la théorie des cyclones. *Proc.-verb. Assoc. Météor. U.G.G.I. (Edinburgh), Pt. II (Mém.)*, 66–82.

Stone, P. H., 1966: On non-geostrophic baroclinic stability. *J. Atmos. Sci.*, **23**, 390–400.

——, S. Hess, R. Hadlock and P. Ray, 1969: Preliminary results of experiments with symmetric baroclinic instabilities. *J. Atmos. Sci.*, **26**, 991–996.